Highly Efficient Remediation of Chloridazon and Its Metabolites

Yan, Feng; Kumar, Sumit; Spyrou, Konstantinos; Syari'ati, Ali; De Luca, Oreste; Thomou, Eleni; Alfonsín, Estela Moretón; Gournis, Dimitrios; Rudolf, Petra

Published in:
ACS Environmental Science and Technology Water

DOI:
10.1021/acsestwater.0c00037

Publication date:
2021

ACS ES&T Water

pubs.acs.org/estwater

Article

Highly Efficient Remediation of Chloridazon and Its Metabolites: The Case of Graphene Oxide Nanoplatelets

Feng Yan, Sumit Kumar, Konstantinos Spyrou, Ali Syari'ati, Oreste De Luca, Eleni Thomou, Estela Moretón Alfonsín, Dimitrios Gournis, and Petra Rudolf*

Cite This: *ACS EST Water* 2021, 1, 157–166

Read Online

ACCESS | Metrics & More | Article Recommendations | Supporting Information

ABSTRACT: The contamination of aqueous environments by aromatic pollutants has become a global issue. Chloridazon, a herbicide considered as harmless to the ecosystem, has been widely used in recent decades and has accumulated, together with its degradation products desphenyl-chloridazon and methyl-desphenyl-chloridazon, to a non-negligible level in surface water and groundwater. To respond to the consequent necessity for remediation, in this work, we study the adsorption of chloridazon and its metabolites by graphene oxide and elucidate the underlying mechanism by X-ray photoelectron spectroscopy. We find a high adsorption capacity of 67 g kg^{-1} for chloridazon and establish that bonding of chloridazon to graphene oxide is mainly due to hydrophobic interaction and hydrogen bonding. These findings demonstrate the potential of graphene-based materials for the remediation of chloridazon and its metabolites from aqueous environments.

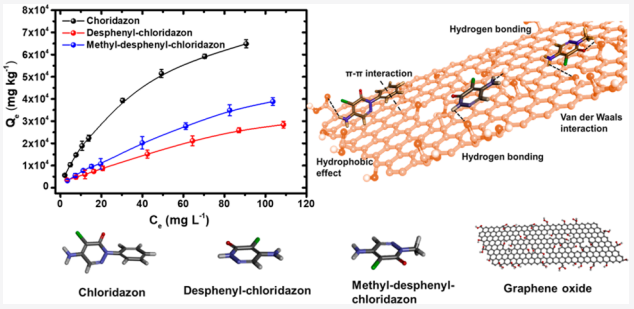

KEYWORDS: *graphene oxide, chloridazon and its metabolites, environmental remediation, adsorption mechanism, X-ray photoelectron spectroscopy*

INTRODUCTION

The occurrence of organic micropollutants, such as herbicides, in the groundwater has attracted global attention, given the potential negative effects on human health.[1,2] Chloridazon, a herbicide that inhibits the photosynthesis process in annual broad-leaf weeds, has been widely used in the past several decades because it was considered as relatively harmless.[3,4] The degradation of chloridazon generates two metabolites, desphenyl-chloridazon and methyl-desphenyl-chloridazon.[5,6] Due to their polarity and solubility, they are regarded as mobile compounds, which cause surface water and groundwater pollution.[7] European regulations impose the maximum residue limit for herbicide/pesticide concentrations in groundwater of 0.1 $\mu g\ L^{-1}$ for single compounds and 0.5 $\mu g\ L^{-1}$ for the sum of all herbicides and pesticides,[8] but the concentration of chloridazon in some parts of Europe has arrived at 3.5 $\mu g\ L^{-1}$, substantially exceeding the concentration limits. Moreover, the major metabolite, desphenyl-chloridazon, was present in natural water at a concentration of 24.0 $\mu g\ L^{-1}$, while the other metabolite, methyl-desphenyl-chloridazon, was found at a concentration of 6.1 $\mu g\ L^{-1}$.[6] Although the metabolites, desphenyl-chloridazon and methyl-desphenyl-chloridazon, are not active as herbicides[9] and classified as nonrelevant metabolites in Germany,[10] the accumulation and persistence in water may have potentially negative effects on human health. Activated carbon (AC) is currently deemed the most efficient material for herbicide remediation from drinking water because it achieves removal of ≤90% of herbicides.[11] However, there are some disadvantages that need to be considered, such as bacterial contamination,[12] high-energy consumption in the regeneration process, and most importantly the high commercial cost for producing precise surface properties and for operating the regeneration process.[13] It is imperative to develop an effective and relatively low-cost technology to prevent the concentration of chloridazon and its metabolites in drinking water from exceeding acceptable limits.

Graphene oxide, a two-dimensional material composed of sp^2-hybridized carbon in a planar network decorated with oxygen-containing groups, has attracted considerable attention in water purification in recent years.[14−17] Due to the large amount of epoxy, hydroxyl, and carboxyl groups present on the surface and at the edges of the sheets, graphene oxide (GO) shows hydrophilic properties and can therefore be applied in the aqueous environment for remediation of pollutants[18−20] through filtration,[21,22] catalytic degradation,[23,24] and adsorp-

Received: June 17, 2020
Revised: September 19, 2020
Accepted: September 21, 2020
Published: September 28, 2020

tion.[25,26] Among these techniques, adsorption has been found to be one of the most effective methods because of its wide adaptability, ease of operation, and relatively low cost.[27] Water-soluble organic pollutants with aromatic rings and cationic atoms are particularly favorable for adsorption on GO through $\pi-\pi$ stacking and ionic interaction. For instance, Pei et al.[28] demonstrated that graphene oxide has an excellent adsorption capacity for four aromatic organic compounds (TCP, TCB, 2-naphthol, and naphthalene) and showed that $\pi-\pi$ interaction and hydrogen bonding both play an important role in the adsorption process. Yang et al.[29] investigated the possibility of removal of differently charged organic pollutants from water by GO and found an excellent adsorption capacity toward positively charged compounds, while for negatively charged compounds, the adsorption capacity was relatively low. These results highlight the potential of GO as a suitable adsorbent for organic pollutants. However, to the best of our knowledge, its potential for application in the remediation of chloridazon and its metabolites has not been investigated.

To better evaluate the potential of graphene oxide for adsorbing chloridazon and its metabolites from an aqueous environment, in this work batch equilibration experiments were performed to unravel the physicochemical adsorption properties. In addition, in view of further improvement of the sorbent's performance and possibly industrial application, we employed X-ray photoelectron spectroscopy to gain insight into the adsorption mechanism of chloridazon and its metabolites on graphene oxide.

EXPERIMENTAL SECTION

Materials. Graphite flakes (<20 μm) were obtained from Sigma-Aldrich. Sulfuric acid (H_2SO_4, 95−97%, AR) and nitric acid (HNO_3, 65%, AR) were purchased from Boom BV. Potassium chlorate ($KClO_3$, ≥99.0%, AR) and chloridazon ($C_{10}H_8ClN_3O$, AR) were acquired from Sigma-Aldrich. Desphenyl-chloridazon ($C_4H_4ClN_3O$, AR) and methyl-desphenyl-chloridazon ($C_5H_6ClN_3O$, AR) were purchased from Enamine Ltd. All chemicals were used without further purification.

Characterization of Materials. The morphology of the graphene oxide sheets was observed using atomic force microscopy (AFM) and transmission electron microscopy (TEM). AFM was performed on a Digital Nanoscope V Multimode instrument (Digital Instruments, Santa Barbara, CA) in tapping mode, while TEM images were collected with a Fei Nova 650 instrument, operated at an acceleration voltage of 30 kV. FTIR spectra in the range of 4000−500 cm^{-1} were recorded on KBr pellets containing 2 wt % GO on a Shimadzu 8400 infrared spectrometer; each spectrum reported is the sum of 200 scans and was collected with the resolution set to 2 cm^{-1}. X-ray diffraction (XRD) patterns were acquired using a D8 Advance Bruker diffractometer with Cu Kα radiation (λ = 1.5406 Å) employing a 0.25° divergent slit and a 0.125° antiscattering slit; the 2θ scattered intensity was recorded in the range from 2.00° to 80.00° in steps of 0.02° and a counting time of 2 s per step. Raman spectra were recorded with a micro-Raman system RM 1000 RENISHAW, with excitation at 532 nm, in the range of 1000−2400 cm^{-1}; the size of the laser spot was 1 μm, and a low laser power of 1 mW was used to prevent overheating of the sample. Dynamic light scattering (DLS) measurements were performed on a Malvern Zetasizer Nano ZS90 system with a diode laser with a wavelength of 633 nm; a GO/water suspension with a GO concentration of 0.25 wt % was placed in the latex cell and measured at a detector angle of 173°, a refractive index of 1.3, and a temperature of 25 °C. The ζ potential of graphene oxide or graphene oxide with chloridazon and its metabolites adsorbed was determined in an aqueous solution with a concentration of 0.05 mg mL^{-1} with a ZetaPALS instrument (Brookhaven Instruments Co., Helts-ville, NY) using Uzgiris electrodes coated with palladium; all of the samples were measured five times in 10 mm polystyrene cuvettes. X-ray photoelectron spectroscopy (XPS) was performed with a model SSX-100 (Surface Science Instruments) photoelectron spectrometer, equipped with a monochromatic Al Kα X-ray source ($h\nu$ = 1486.6 eV) and operating at a pressure of 1×10^{-9} mbar. The samples were dispersed in water by being stirred for 1 h, and a small drop of the suspension was left to dry in air on a 150 nm thick gold film supported on mica.[30] The photoelectron takeoff angle was 37° with respect to the surface normal. The analyzed spot size on the sample was 600 μm in diameter. The experimental resolution was set to 1.67 eV for overview spectra and to 1.26 eV for the detailed scans of the various core level regions. Binding energies are reported ±0.1 eV and referenced to the $Au4f_{7/2}$ level at 84.0 eV.[31] All XPS spectra were analyzed using the least-squares curve-fitting program Winspec (developed at LISE, University of Namur, Namur, Belgium). Deconvolution of the spectra included a Shirley background[32] subtraction and fitting with a minimum number of peaks consistent with the chemical structure of the sample, taking into account the experimental resolution. For the N1s line, a linear background subtraction was employed because the low peak intensity did not allow for Shirley background subtraction. The profile of the peaks was taken as a convolution of Gaussian and Lorentzian functions. The uncertainty in the peak intensity determination is 2% for all core levels reported.

Synthesis of Graphene Oxide Nanosheets. Graphene oxide nanosheets were synthesized from graphite flakes using a modified Staudenmaier's method, which was also applied in our previous work.[25,33] In detail, 5 g of graphite powder was added to a glass beaker, which contained concentrated sulfuric acid (200 mL) and nitric acid (100 mL), while cooling in an ice/water bath. Then, 200 g of potassium chlorate powder was added to the mixture in small portions while it was being cooled and stirred. The oxidation reaction was quenched after 18 h by pouring the viscous mixture into a large amount of distilled water; the product was precipitated and washed until a pH of 6.0 was reached. Graphene oxide was obtained after centrifugation (5000 rpm, 10 min) and spreading on glass plates for air drying.

Batch Adsorption Experiments. Milli-Q water (resistivity of 18 MΩ cm, 25 °C) was used in the adsorption experiment. Ten milligrams of graphene oxide was dispersed in 10 mL of water by being magnetically stirred for 24 h in a glass vial. Stock solutions of 250 ppm chloridazon, desphenyl-chloridazon, and methyl-desphenyl-chloridazon were prepared in Milli-Q water. Batch adsorption experiments were conducted in a water bath at different constant temperatures (25, 35, 45, 55, and 65 °C) on a hot plate while being stirred with a speed set to 200 rpm. Chloridazon, disphenyl-chloridazon, or methyl-desphenyl-chloridazon was added, at diluted concentrations from 5 to 125 ppm, to 10 mL of a homogeneously dispersed graphene oxide suspension. The suspensions were stirred continuously for 24 h to ensure that the adsorption equilibrium was achieved. The pH of the mixture was adjusted to 6.0 ± 0.1 (close to natural water) by

https://dx.doi.org/10.1021/acsestwater.0c00037
ACS EST Water 2021, 1, 157−166

adding 0.1 M NaOH and measured before the batch adsorption experiment was started and after the adsorption equilibrium was achieved to verify that the pH was stable during the experiment. The suspensions were centrifuged at 12000 rpm, and the supernatant was filtered with 0.45 μm nylon filters. The concentrations of chloridazon and its metabolites were measured by high-performance liquid chromatography (Prominence HPLC, Shimadzu) using a diode array detector and data station and analyzed at 283 nm,[34,35] the wavelength of maximum adsorption of those compounds. The calibration curves of three compounds are shown in Figure S1. All of the experimental data reported are the average of triplicate determinations.

The adsorption capacities Q_e (milligrams per kilogram) of the molecule on the sorbent were determined by eq 1:

$$Q_e = [(C_0 - C_e)/m] \times V \quad (1)$$

where C_0 (milligrams per liter) and C_e (milligrams per liter) are the initial and equilibrium concentrations, respectively, m (kilograms) is the mass of graphene oxide used in the batch adsorption experiment, and V (liters) represents the volume of the suspension. The removal efficiency was calculated by the following equation:

$$\text{removal}\,(\%) = [(C_0 - C_e)/C_0] \times 100\% \quad (2)$$

Isotherm Models. The adsorption isotherm describes how the adsorbed molecules are distributed between the liquid and the solid phase, when the adsorption reaches an equilibrium state. The adsorption data were fitted with the two most used models to describe adsorption isotherms, the Freundlich and Langmuir models. The parameters obtained from the two models provide important information about the adsorption mechanism as well as on the affinity of the sorbent. The Freundlich model[36] relates the solute concentration to the adsorbent surface affinity and is written as

$$\ln Q_e = \ln K_f + 1/n \ln C_e \quad (3)$$

where Q_e (milligrams per kilogram) is the adsorption capacity at the equilibrium state, C_e (milligrams per liter) is the concentration of chloridazon and its metabolites in the equilibrium state, and K_f [mg kg^{-1} (mg L^{-1})$^{-n}$] is the Freundlich constant, which indicates the affinity of the adsorbate for the sorbent. The parameter n takes into account the surface heterogeneity of the adsorbent; n is the heterogeneity factor, which represents the bond distribution.

The Langmuir isotherm[37] assumes a surface with homogeneous binding sites, equivalent sorption energies, and no interaction between adsorbates. The linear form, which applies when no dissociation upon adsorption takes place, is written as

$$1/Q_e = 1/q_m + 1/K_L q_m C_e \quad (4)$$

where Q_e (milligrams per kilogram) is the adsorption capacity at equilibrium, q_m (milligrams per kilogram) is the maximum adsorption capacity of the sorbent in the equilibrium state, C_e (milligrams per liter) is the concentration of chloridazon or its metabolites at equilibrium, and K_L (liters per milligrams) is the binding constant related to the strength of the sorbent−adsorbate interaction.

RESULTS AND DISCUSSION

Characterization of Graphene Oxide. First, it is important to verify the composition, structure, and morphology of the sorbent. The characterization data of our GO are reported in the Supporting Information and agree with other batches documented in our previous publications.[25,33] The morphology of the exfoliated GO sheets was observed by AFM (Figure S2a) and TEM (Figure S2c,d), which present winkles and defects located on the edges, and the fact that their thickness is around 1 nm, suggesting the graphene oxide was exfoliated into single sheets.[38] The color of a graphene oxide suspension (0.5 mg mL^{-1} in Milli-Q water) was brownish yellow as shown in Figure S2d, and the average size was confirmed as ∼5 μm by DLS (Figure S2b). The X-ray diffraction pattern, presented in Figure S2f, revealed a peak centered at 11.4 ± 0.1°, which corresponds to the (002) diffraction and an interlayer spacing of 8.3 ± 0.1 Å. The Raman spectrum (Figure S2g) shows two strong peaks, one centered at 1580 cm^{-1} (G band) and attributed to the vibration of sp^2-bound carbon atoms and another located at 1350 cm^{-1} (D band), deriving from the presence of sp^3-hybridized carbon, i.e., the oxygen-containing functional groups. The latter can be identified from the Fourier-transform infrared (FTIR) spectrum in Figure S3a, via the IR bands due to stretching vibrations. In fact, the FTIR spectrum testifies to the existence of aromatic C═C (1620 cm^{-1}), epoxy C−O (1220 cm^{-1}), carboxyl O═C−O (1390 cm^{-1}), and alkoxy C−O (1054 cm^{-1}) groups; the broad peak centered at 3400 cm^{-1} is ascribed to the −OH stretching vibration.

X-ray photoelectron spectroscopy (XPS) allows instead the quantification of the relative abundance of the various oxygen-containing groups, because the spectral intensity is directly proportional to the atomic percentage (at. %) of the element in a particular chemical environment. The wide scan spectrum in Figure S3b shows two peaks centered at 285.0 and 530.0 eV in binding energy (BE) and stemming from carbon and oxygen, respectively. The ratio of the total intensities of the C1s to O1s photoemission lines for graphene oxide was calculated to amount to 1.65 ± 0.04, corresponding to an oxygen content of 37.7 ± 0.6 at. %. In the detailed C1s spectrum of GO, presented in Figure S3c, at least four contributions can be distinguished. The first, which peaked at 285.0 eV in BE, derives from C−C bonds of the hexagonal structure and represents 25.0% of the total C1s intensity. The most intense contribution, centered at a BE of 287.2 eV, is due to the carbonyl (C═O) and epoxy (C−O) functional groups and accounts for 46.0% of the total carbon spectral intensity. The peaks at BEs of 285.8 and 288.3 eV arise form C−O and C(O)O bonds and account for 17.0% and 10.0% of the C1s intensity, respectively. These percentages match up with those of our previous batches.[25,33]

Effect of Temperature on the Adsorption of Chloridazon and Its Metabolites. Once sure of the quality of the sorbent, we started with the adsorption experiments. The temperature of the system is an important factor when exploring the thermodynamics of the adsorption process. The influence of the solution temperature on the chloridazon, desphenyl-chloridazon, and methyl-desphenyl-chloridazon adsorption capacities of graphene oxide is shown in Figure 1a. The adsorption capacities were found to decrease with an increase in temperature in the range of 25−65 °C, which indicates that the adsorption of chloridazon, desphenyl-chloridazon, and methyl-desphenyl-chloridazon on graphene oxide is an exothermic process;[39] in other words, the creation of a bond between adsorbate (chloridazon and its metabolites) and GO is accompanied by the release of heat. The removal

https://dx.doi.org/10.1021/acsestwater.0c00037
ACS EST Water 2021, 1, 157−166

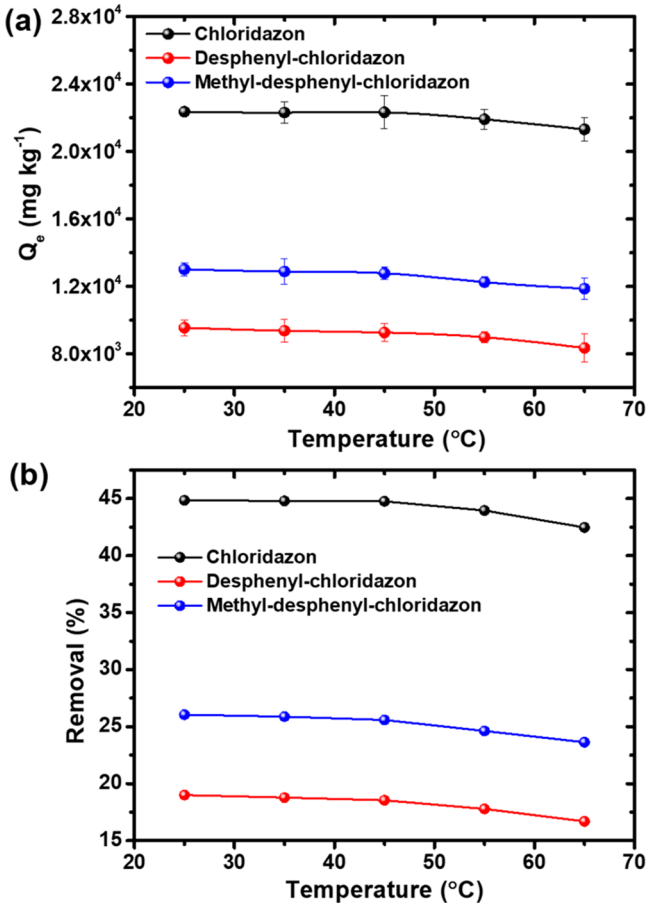

Figure 1. Effect of temperature on the (a) adsorption capacity and (b) removal efficiency for adsorption of chloridazon, desphenyl-chloridazon, and methyl-desphenyl-chloridazon on graphene oxide.

efficiencies of chloridazon and its metabolites by graphene oxide, calculated with the help of eq 2 and illustrated in Figure 1b, decrease in the following order: chloridazon > methyl-desphenyl-chloridazon > desphenyl-chloridazon. Specifically, the efficiency of chloridazon removal by GO was determined to be 42.5−44.9%, which is much higher than that for methyl-desphenyl-chloridazon (23.6−26.1%) and desphenyl-chloridazon (16.7−19.2%) in this temperature range.

Adsorption Isotherms. The adsorption isotherms of chloridazon, desphenyl-chloridazon, and methyl-desphenyl-chloridazon on graphene oxide were obtained for a range of initial concentrations from 5 to 125 mg L^{-1} and are presented in Figure 2a. They all belong to class L of the classification by Giles, Smith, and Huitson based on the differences in the relative magnitude of the activation energies of desorption of solutes and solvent.[40] This indicates that as coverage increases, it becomes more and more difficult for chloridazon or its metabolites to find a vacant adsorption site. In the initial part of the isotherms, the slope of the curve for chloridazon is significantly higher than that of desphenyl-chloridazon and of methyl-desphenyl-chloridazon, which points to a higher affinity of chloridazon for graphene oxide than of desphenyl-chloridazon and methyl-desphenyl-chloridazon. As a result, at an initial concentration of 125 mg L^{-1}, the adsorption capacity for chloridazon reached 64880 mg kg^{-1}, while the adsorption capacities for desphenyl-chloridazon and methyl-desphenyl-chloridazon were found to amount to 28335 and 38806 mg kg^{-1}, respectively.

The removal percentages of chloridazon and its metabolites as a function of adsorbate (chloridazon, desphenyl-chloridazon, or methyl-desphenyl-chloridazon) dosage, collected under the exact same conditions with a sorbent (graphene oxide) concentration of 500 mg L^{-1}, are shown in Figure 2b. For all three compounds, the removal efficiency decreased with an increase in the initial concentration; specifically, the removal efficiency for chloridazon was 56.2% at the initial concentration of 5 mg L^{-1}, while it was reduced to 27.6% at the initial concentration of 125 mg L^{-1}. This is expected because the number of adsorption sites on graphene oxide is limited, and when the chloridazon concentration is higher, a lower percentage of the molecules present in solution can find an empty site on which to adsorb. Interestingly, the affinity of desphenyl-chloridazon for GO was significantly increased when the initial concentration was <15 mg L^{-1}, and consequently, under these conditions, the removal efficiency of desphenyl-chloridazon surpassed that of methyl-desphenyl-chloridazon and reached 34.8%.

The isotherms were fitted with the Freundlich and Langmuir isotherm equations to describe the adsorption behaviors of graphene oxide with chloridazon and its metabolites, as shown in panels c and d of Figure 2. The fitting was performed with Origin Lab software, and the results are listed in Table 1. For the Freundlich model, the R^2 values amounted to 0.992 for chloridazon, 0.979 for desphenyl-chloridazon, and 0.998 for methyl-desphenyl-chloridazon, confirming the good quality of the fits. The values of n, the parameter that relates to the heterogeneity of the sorbent surface, were close for chloridazon, desphenyl-chloridazon, and methyl-desphenyl-chloridazon, indicating that the surface properties of graphene oxide dominate the adsorption process. The empirical constant K_f for chloridazon was almost 3 times those of desphenyl-chloridazon and methyl-desphenyl-chloridazon, which confirms that chloridazon has a higher affinity for GO than its two metabolites. Also in the case of the fitting based on the Langmuir model, the R^2 values point to a good fit. The q_m and K_L values are higher for chloridazon than for its metabolites, pointing to a stronger interaction between graphene oxide and the former, which is consistent with the result from the fitting with the Freundlich model. The maximum adsorption capacity q_m was determined to be 67180 mg kg^{-1} for chloridazon, 34299 mg kg^{-1} for desphenyl-chloridazon, and 36849 mg kg^{-1} for methyl-desphenyl-chloridazon. As one can see in Table 2, compared to other sorbents reported in the literature, our result for chloridazon is high but does not exceed that for adsorption on active carbon, the most frequently employed, commercially available sorbent for remediation of this herbicide. For the remediation of the metabolites desphenyl-chloridazon and methyl-desphenyl-chloridazon, we could not find reported values except in our previous work.[41]

Comparative Analysis of the Environmental Impact for Graphene Oxide and Activated Carbon. Because the adsorption capacity of graphene oxide for chloridazon was found to be only 10% lower than that of activated carbon (AC), which is the currently used commercial sorbent, it is worth comparing these two sorbents for what concerns environmental impact to decide whether graphene oxide should be optimized and further developed arrive at a commercially competitive sorbent for remediation of chloridazon and other pollutants from aqueous environments. The standard methodology for the comparison of the environmental impact is the life cycle assessment (LCA), but we have

https://dx.doi.org/10.1021/acsestwater.0c00037
ACS EST Water 2021, 1, 157−166

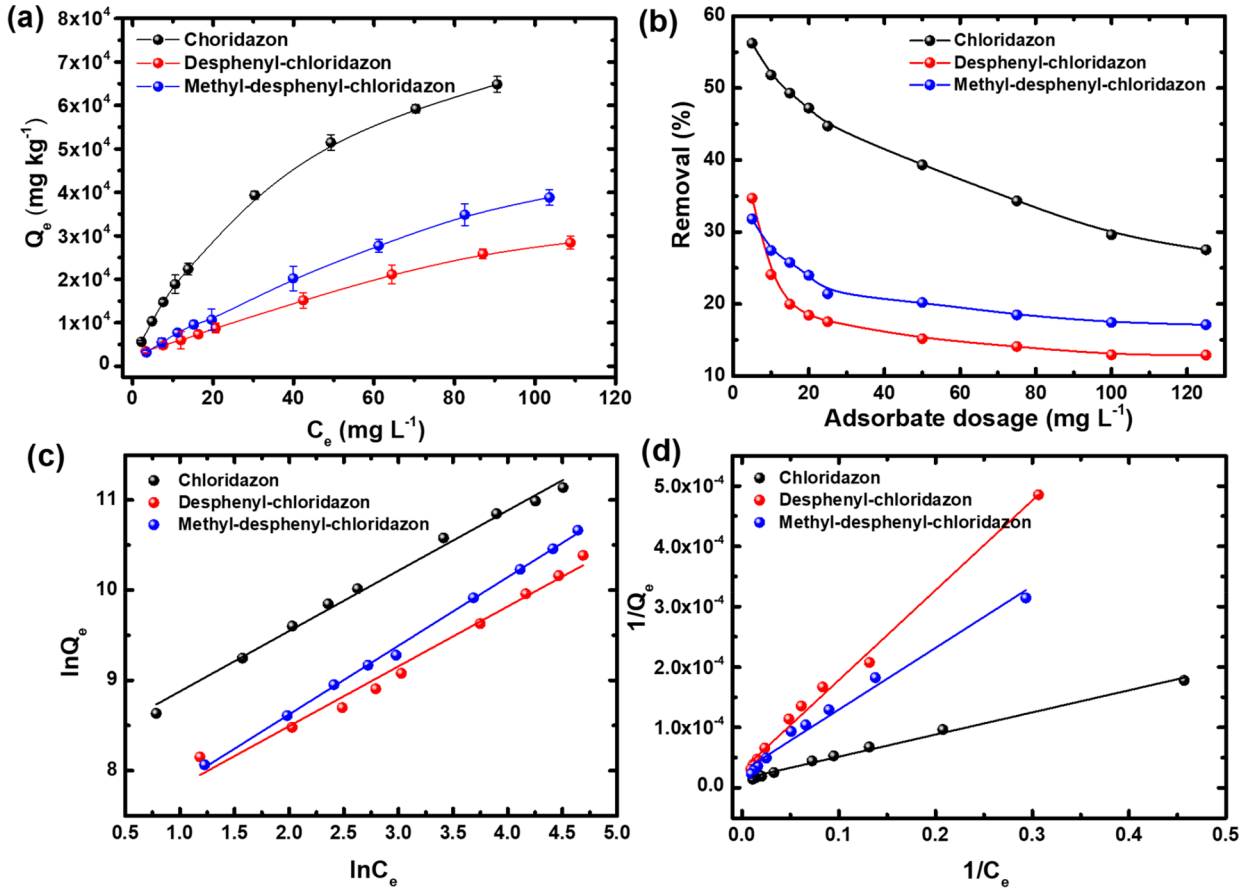

Figure 2. (a) Adsorption isotherms of chloridazon, desphenyl-chloridazon, and methyl-desphenyl-chloridazon on graphene oxide. (b) Effect of adsorbate dosage on the removal efficiency of the adsorptions. Same data as in panel a plotted according to the (c) Freundlich and (d) Langmuir adsorption isotherm models for chloridazon, desphenyl-chloridazon, and methyl-desphenyl-chloridazon on graphene oxide at room temperature.

Table 1. Parameters of the Freundlich and Langmuir Models for the Adsorption of Chloridazon, Desphenyl-chloridazon, and Methyl-desphenyl-chloridazon on Graphene Oxide

	Freundlich			Langmuir		
adsorbate	K_f [mg kg^{-1} (mg L^{-1})$^{-n}$]	n	R^2	q_m (mg kg^{-1})	K_L (L mg^{-1})	R^2
chloridazon	3671.19	1.494	0.992	67180	0.0406	0.993
desphenyl-chloridazon	1296.34	1.509	0.979	34299	0.0195	0.992
methyl-desphenyl-chloridazon	1214.76	1.315	0.998	36849	0.0267	0.981

Table 2. Parameters of the Freundlich and Langmuir Models for the Adsorption of Chloridazon, Desphenyl-chloridazon, and Methyl-desphenyl-chloridazon on Graphene Oxide

adsorbent	adsorption capacity (mg kg^{-1})	initial concentration range (ppm)	temperature (°C)	pH	ref
kerolite	288	2.3−40.0	25	[a]	42
sepiolite-600	164	1.0−200.0	25	[a]	43
ammonium kerolite	21274	8.5−254.8	25	[a]	44
kerolite-600	2253	1.0−200.0	25	7.4	45
Cu^{2+}@POSS_SWy-2	4920	5.0−25.0	25	[a]	41
activated carbon	75600	0.1−0.5	25	8.2	46
MSNPs/PANI	3000	2.0−100.0	25	7.0	47
graphene oxide	67180	5.0−125.0	25	6.0	this work

[a]pH not available.

not been able to find a comparative LCA study of activated carbon and graphene oxide for water treatment in the literature. However, existing publications can help in answering the question of which of the two materials is the more environmentally friendly option in the long run.

There are three main stages to consider in the life cycle of these materials: production, utilization, and end of life. Kozyatnyka et al.[48] studied three carbonaceous materials for water treatment up to the end of life: AC (fossil-based activated carbon), BC (biochar), and HC (hydrochar), where

https://dx.doi.org/10.1021/acsestwater.0c00037
ACS EST Water 2021, 1, 157−166

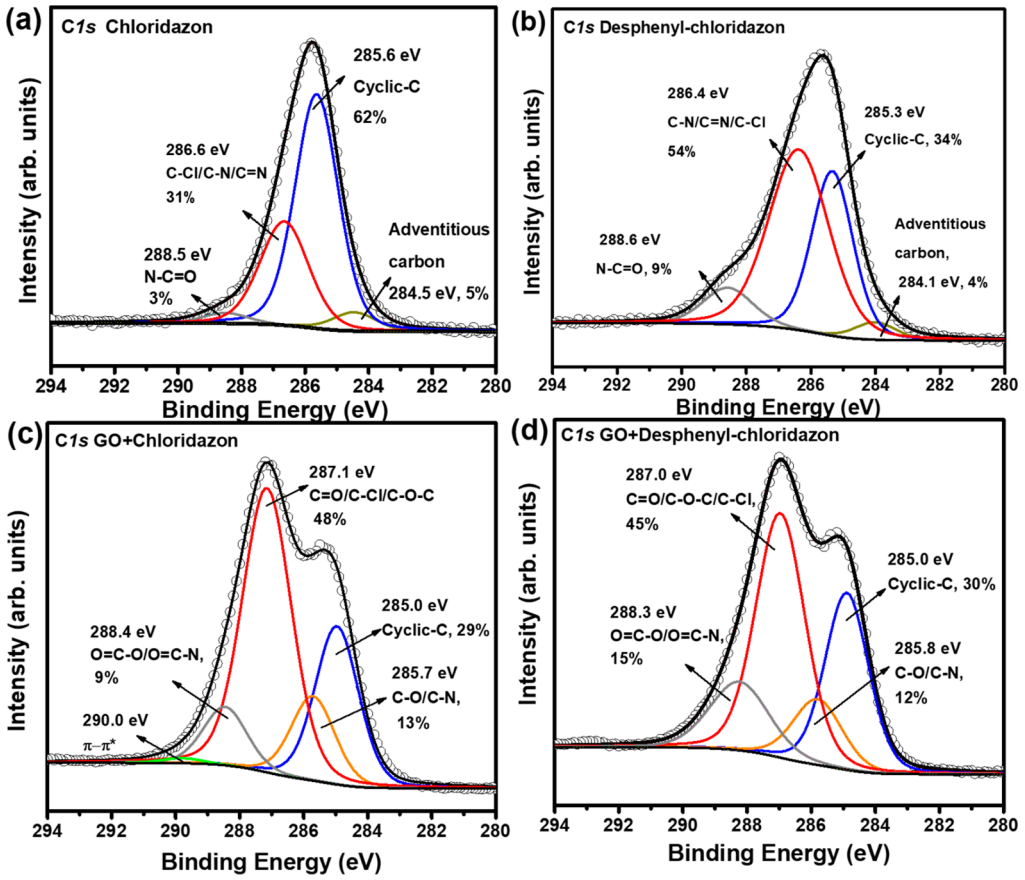

Figure 3. X-ray photoelectron spectroscopy of the C1s core level region of (a) chloridazon, (b) desphenyl-chloridazon, (c) chloridazon adsorbed on graphene oxide, and (d) desphenyl-chloridazon adsorbed on graphene oxide.

the last two are biobased. They simulated three scenarios for each material's end of life (incineration, regeneration, and landfilling) and found for all three materials, the regeneration stage to be the best scenario, with AC having a weaker impact because of its larger pore volume, which implies less material for the same performance.

For the production of GO, there are different synthesis pathways whose environmental footprint has been analyzed.[49] This LCA comparative study considers the impact of the main three routes for graphene production (CVD, electrochemical exfoliation, and chemical oxidation with chemical/thermal reduction) and simulates the implementation of industrial production for each synthetic process, finding a great decrease in the environmental impact as compared to laboratory production conditions. The results show that of the three, chemical oxidation has the weakest impact; the Staudenmaier method used in our work falls in this category.

Finally, Cossutta et al.[50] have compared graphene and AC for supercapacitor applications. They found that the production of the supercapacitor components and the use stage have very little effect compared with the production stage of the active materials. At the production stage, graphene was found to have 2.5 times the impact of AC. When the end of life is included, the impact of graphene sees a reduction of >80% as compared to AC. Overall, however, graphene still has 1.5 times more impact than AC, but after application of the theoretical values of the total capacitance of graphene (technological advancement coefficient), graphene becomes less impactful than AC. When these authors simulated the production in a decarbonized energy scenario, this difference grows even larger. Even though Cossutta and co-workers consider the capacitance of the materials and not their adsorbance, a parallel can be drawn for our case because active carbone is a more mature technology for water remediation than GO, but also has less potential for improvement. In conclusion, the sources used to produce AC have very little impact as compared with the pore volume and surface area of the material. The chemical oxidation process used for the synthesis of GO in this study is the most sustainable of the existing production routes. In addition, finally, even though the impact of GO is stronger than that of AC as of now, if industrial production and/or theoretical performance is achieved, it has the potential to be less impacting. When these technological advancements are considered in a decarbonized energy scenario, the advantage of GO over AC increases.

Adsorption Mechanism. To reveal the underlying adsorption mechanism of chloridazon and its metabolites on graphene oxide, X-ray photoelectron spectroscopy (XPS) was performed to gain insight into the bonding between the molecules and GO. Organic molecules can usually adsorb on graphene-based materials via the hydrophobic effect,[51,52] $\pi-\pi$ interaction,[53,54] hydrogen bonding,[28,55] electrostatic interactions,[29,56] and van der Waals interaction.[57,58]

Hydrophobic interaction has been identified as being most important for the adsorption of hydrophobic and nonpolar organic molecules on graphene-based materials, even if the classification of graphene as hydrophilic or hydrophobic depends very much on the environment.[59] Graphene oxide

https://dx.doi.org/10.1021/acsestwater.0c00037
ACS EST Water 2021, 1, 157−166

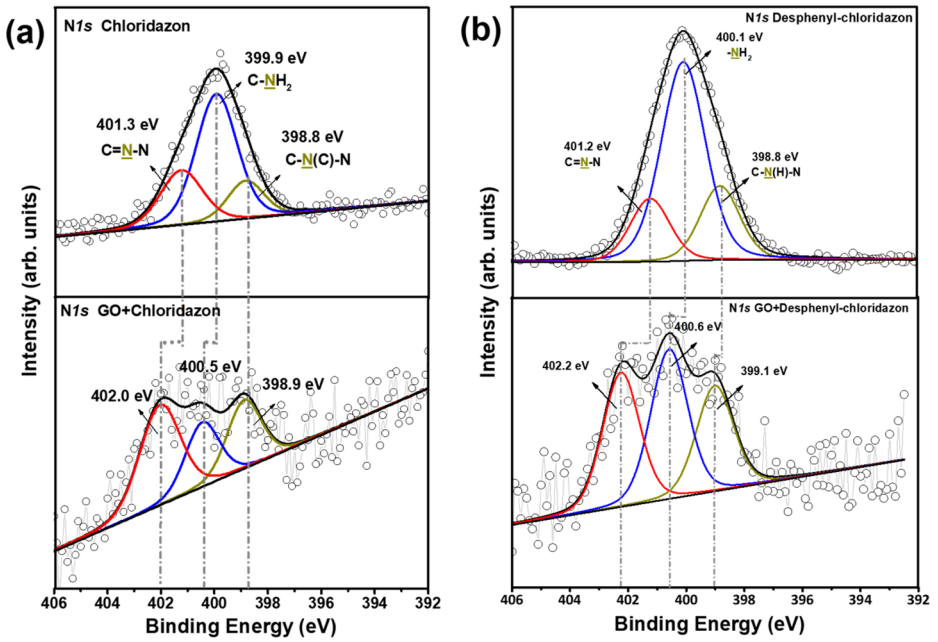

Figure 4. X-ray photoelectron spectra of the N1s core level region of (a) chloridazon and graphene oxide with chloridazon and (b) desphenyl-chloridazon and graphene oxide with desphenyl-chloridazon.

to some extent can be identified as amphiphilic because it contains hydrophilic oxygen-containing groups and hydrophobic polyaromatic islands on the basal plane,[60] which still have affinity for nonpolar molecules. A parameter related to the hydrophobicity or hydrophilicity of organic molecules is the octanol/water partition coefficient, K_{ow}, defined as the ratio of the compound's concentration in octanol to its concentration in the aqueous phase of a two-phase octanol/water system.[61] As shown in Table S1, the $\log K_{ow}$ of chloridazon (1.19) is higher than those of desphenyl-chloridazon (−1.59) and methyl-desphenyl-chloridazon (−1.37), and its water solubility is much lower (442 mg L^{-1}), meaning that chloridazon has a higher affinity for the hydrophobic polyaromatic islands of GO.[52] Hence, the hydrophobic character of chloridazon could be the cause for its superior affinity for GO.

To explore the role of $\pi-\pi$ and hydrogen bonding interactions in the adsorption process, XPS was employed. Four different types of carbon bonds contribute to the C1s core level photoemission spectra of chloridazon, shown in Figure 3a, and desphenyl-chloridazon, shown in Figure 3b. These are cyclic C, found at BEs of 285.3−285.6 eV; adventitious carbon from the exposure to air, typically situated at 284.5 eV; C−Cl, C−N, and C═N giving rise to the spectral intensity in the BE range of 286.4−286.6 eV; and N−C═O, the component with the highest BE of 288.5 eV.[59]

If one compares the C1s core level photoemission spectra of the as-prepared GO discussed above (Figure S2c) with the one collected after adsorption of chloridazon, shown in Figure 3c or of desphenyl-chloridazon Figure 3d, one notes that the relative intensity of the component due to O═C−O/O═C−N is significantly higher in the latter spectra. That indicates that chloridazon and desphenyl-chloridazon both have been successfully adsorbed on graphene oxide. The $\pi-\pi^*$ shake-up at 290.0 eV is visible only for chloridazon adsorbed on the graphene oxide surface (Figure 3c) because chloridazon has an extra phenyl ring where desphenyl-chloridazon has a H instead.[62,63] The oxygen-containing groups of graphene oxide are a source of hydrophilicity. These groups interrupt the sp^2-hybridized structure,[64] so that the $\pi-\pi^*$ shake-up satellite peak represents almost 1% of the total carbon intensity. This implies that there is not enough sp^2-hybridized carbon for the $\pi-\pi$ interaction to be the dominating mechanism for adsorption.

The XPS spectra of the N1s core level region of chloridazon and desphenyl-chloridazon and of the same molecules adsorbed on graphene oxide are presented in Figure 4. The N1s spectra of chloridazon and desphenyl-chloridazon molecules contain three contributions. The first, which peaked at a BE of 398.8 eV, derives from nitrogen in C−N(C)−N bonds;[65] the second one at a BE of 400.0 eV stems[66] from $-NH_2$, and the third, at a BE of 401.2 eV, corresponds[67] to C═N−N. The latter two components are shifted to higher binding energies by 0.6 and 0.7 eV, respectively, when chloridazon is adsorbed on GO (Figure 4a, bottom panel). Similarly, the components due to $-NH_2$ and C═N−N bonds are shifted 0.5 and 1.0 eV, respectively, to higher BE when desphenyl-chloridazon is adsorbed on GO (Figure 4b, bottom panel). These shifts are due to the formation of a hydrogen bond involving the $-NH_2$ group and to the fact that the C═N−N group on GO creates a resonance structure, which results in electron poor N.[67,68] In chloridazon, the C−N(C)−N group is linked to a benzene ring, which saturates the electron density of the corresponding N; adsorption does not induce any change in this, so the BE of the contribution of the C−N(C)−N group is the same after adsorption on GO. In desphenyl-chloridazon, the C−N(C)−N group bears a -H, which supports the formation of a hydrogen bond to GO, and hence, the N in this group becomes more electron deficient, which in turn results in a 0.3 eV shift toward a higher BE of the corresponding component in the N1s line.

Electrostatic interactions between the molecules in aqueous and GO can be ruled out on the basis of the pK_a values of chloridazon and desphenyl-chloridazon reported in Table S1, which imply that the nitrogen-containing groups in chloridazon and its metabolites cannot be protonated as required for such a bonding interaction. The absence of a component corresponding to protonated N in the N1s core level spectral

https://dx.doi.org/10.1021/acsestwater.0c00037
ACS EST Water 2021, 1, 157−166

of chloridazon with graphene oxide and desphenyl-chloridazon with graphene confirms this scenario. Even though graphene oxide is negatively charged due to the ionization of the carboxylic groups at pH 6.0, there is still no electrostatic interaction between graphene oxide and chloridazon or its metabolites. This can be demonstrated by the ζ potential results shown in Figure S4. The ζ potential values of a graphene oxide aqueous dispersion as a function of pH are in good agreement with those reported previously,[69,70] and the ζ potential of dispersions of graphene oxide with chloridazon or its metabolites adsorbed on the surface shows the same values as bare graphene oxide in the pH range of 6.0−8.0. This implies that these adsorbed molecules have no influence on the surface charge density of graphene oxide.[71] On the contrary, the change in the ζ potential at pH <5.0 is ascribed to the partial ionization of the adsorbed molecules, while the changes for pH >8.0 are thought to stem from the higher ionic strength of NaOH that was used for adjusting the pH of the solution.

van der Waals interactions are relatively weak compared to a chemical bond or a hydrogen bond.[72] As reported by Wang et al.,[73] the size and conformational evolution of the herbicide molecule play an important role for its van der Waals interaction with a graphene oxide sheet. As shown in Table S1, chloridazon obviously has greater steric hindrance than its metabolites. In addition, the rotatable C−C bond in chloridazon can lead to an unconstrained conformational space. Therefore, van der Waals interaction plays a slightly larger role in the adsorption of chloridazon than in that of its two metabolites.

Chloridazon can bind to the graphene oxide surface via hydrogen bonding of the -NH_2 group, while $\pi-\pi$ interaction via the benzene ring plays a limited role. For desphenyl-chloridazon, only hydrogen bonding can contribute to the adsorption on GO. In addition, chloridazon has a stronger van der Waals interaction with and a higher hydrophobic affinity for graphene oxide than desphenyl-chloridazon; because the molecular structures of desphenyl-chloridazon and methyl-desphenyl-chloridazon are similar, the same should hold for both metabolites.

CONCLUSIONS

In this work, graphene oxide was applied for the first time to the remediation of chloridazon and its metabolites from an aqueous environment. A maximum adsorption capacity of 67 g kg^{-1} was found for chloridazon, which is high and comparable to that of the commercial sorbent, activated carbon, which is the most employed for this application. The maximum adsorption capacity of GO for desphenyl-chloridazon was 34 g kg^{-1}, and that for methyl-desphenyl-chloridazon was 37 g kg^{-1}. X-ray photoelectron spectroscopy sheds light on the adsorption mechanism and evidenced that hydrogen bonding between the nitrogen-containing group on chloridazon (or its metabolites) and graphene oxide is the main interaction responsible for the adsorption, while $\pi-\pi$ interaction plays a larger role for chloridazon than for its metabolites. Moreover, chloridazon is also prone to a larger hydrophobic interaction. Because graphene oxide's functional groups can be tailored to enhance its adsorption capacity for chloridazon and other pollutants, in a green economy scenario with a fully decarbonized energy mix and an optimized industrial production of graphene oxide, it becomes the better option than activated carbon from an environmental perspective. Further efforts toward the full exploitation of GO's potential for performance improvement in water remediation are therefore strongly recommended. These should include fabricating graphene oxide into a form where it can adsorb contaminant but not itself disperse into the medium, such as a graphene oxide aerogel, membrane, or magnetic separation.

ASSOCIATED CONTENT

Supporting Information

The Supporting Information is available free of charge at https://pubs.acs.org/doi/10.1021/acsestwater.0c00037.

HPLC calibration curves of chloridazon and its metabolites; AFM, DLS, TEM, XRD, and Raman spectra of graphene oxide; FTIR spectra, wide scan, and C1s core level XPS; ζ potential of graphene oxide and graphene oxide with chloridazon, desphenyl-chloridazon, and methyl-desphenyl-chloridazon adsorbed; a table of selected properties (structure, molecular weight, solubility, $\log K_{ow}$, and pK_a) of chloridazon and its metabolites (PDF)

AUTHOR INFORMATION

Corresponding Author

Petra Rudolf − *Zernike Institute for Advanced Materials, University of Groningen, 9747 AG Groningen, The Netherlands;* orcid.org/0000-0002-4418-1769; Email: p.rudolf@rug.nl

Authors

Feng Yan − *Zernike Institute for Advanced Materials, University of Groningen, 9747 AG Groningen, The Netherlands;* orcid.org/0000-0002-9948-8450

Sumit Kumar − *Zernike Institute for Advanced Materials, University of Groningen, 9747 AG Groningen, The Netherlands*

Konstantinos Spyrou − *Department of Materials Science and Engineering, University of Ioannina, 45110 Ioannina, Greece;* orcid.org/0000-0002-2032-8439

Ali Syari'ati − *Zernike Institute for Advanced Materials, University of Groningen, 9747 AG Groningen, The Netherlands*

Oreste De Luca − *Zernike Institute for Advanced Materials, University of Groningen, 9747 AG Groningen, The Netherlands;* orcid.org/0000-0002-4428-0863

Eleni Thomou − *Zernike Institute for Advanced Materials, University of Groningen, 9747 AG Groningen, The Netherlands; Department of Materials Science and Engineering, University of Ioannina, 45110 Ioannina, Greece;* orcid.org/0000-0002-4253-7987

Estela Moretón Alfonsín − *Zernike Institute for Advanced Materials, University of Groningen, 9747 AG Groningen, The Netherlands*

Dimitrios Gournis − *Department of Materials Science and Engineering, University of Ioannina, 45110 Ioannina, Greece;* orcid.org/0000-0003-4256-8190

Complete contact information is available at: https://pubs.acs.org/10.1021/acsestwater.0c00037

Notes

The authors declare no competing financial interest.

ACKNOWLEDGMENTS

F.Y. gratefully acknowledges the China Scholarship Council (CSC 201704910930) and the University of Groningen for support. A.S. thanks the Indonesian Endowment Fund for

Education (LPDP) for a Ph.D. fellowship. E.T. was supported by the Hellenic Foundation for Research and Innovation (HFRI) and the General Secretariat for Research and Technology (GSRT), under the HFRI Ph.D. fellowship grant (1829). Financial support also came from the Advanced Materials research program of the Zernike National Research Centre under the Bonus Incentive Scheme (BIS) of the Dutch Ministry for Education, Culture and Science. The authors thank Z. Wang and P. J. Deuss for their help with the ζ potential measurements.

REFERENCES

(1) Schwarzenbach, R. P.; Escher, B. I.; Fenner, K.; Hofstetter, T. B.; Johnson, C. A.; Von Gunten, U.; Wehrli, B. The challenge of micropollutants in aquatic systems. *Science* **2006**, *313*, 1072−1077.
(2) Luo, Y.; Guo, W.; Ngo, H. H.; Nghiem, L. D.; Hai, F. I.; Zhang, J.; Liang, S.; Wang, X. C. A review on the occurrence of micropollutants in the aquatic environment and their fate and removal during wastewater treatment. *Sci. Total Environ.* **2014**, *473*, 619−641.
(3) Jakiene, E.; Spruogis, V.; Dautarte, A.; Romaneckas, K.; Avižienytė, D. The bio-organic ano fertilizer improves sugar beet photosynthesis process and productivity. *Zemdirbyste-Agriculture* **2015**, *102*, 141.
(4) Cioni, F.; Maines, G. Weed control in sugarbeet. *Sugar Tech* **2010**, *12*, 243−255.
(5) Buttiglieri, G.; Peschka, M.; Frömel, T.; Müller, J.; Malpei, F.; Seel, P.; Knepper, T. P. Environmental occurrence and degradation of the herbicide n-chloridazon. *Water Res.* **2009**, *43*, 2865−2873.
(6) Schuhmann, A.; Gans, O.; Weiss, S.; Fank, J.; Klammler, G.; Haberhauer, G.; Gerzabek, M. H. A long-term lysimeter experiment to investigate the environmental dispersion of the herbicide chloridazon and its metabolites-comparison of lysimeter types. *J. Soils Sediments* **2016**, *16*, 1032−1045.
(7) European Food Safety Authority (EFSA). Conclusion regarding the peer review of the pesticide risk assessment of the active substance chloridazon. *EFSA J.* **2007**, *5*, No. 108r.
(8) Directive 2006/118/EC of the European Parliament and of the Council of 12 December 2006 on the protection of groundwater against pollution and deterioration. *Official Journal of the European Union* **2006**, *372*, 19−31.
(9) Fischer, A. 1-phenyl-4-amino-5-chlor-pyridazon-6*(PCA) als ein neues Rübenherbizid. *Weed Res.* **1962**, *2*, 177−184.
(10) Guidance document on the assessment of the relevance of metabolites in groundwater of substances regulated under council directive 91/414/EEC. 2003, Sanco/221/2000 -rev.10- final, February, 25, 2003 (https://ec.europa.eu/food/sites/food/files/plant/docs/pesticides_ppp_app-proc_guide_fate_metabolites-groundwtr.pdf).
(11) Ormad, M. P.; Miguel, N.; Claver, A.; Matesanz, J. M.; Ovelleiro, J. L. Pesticides removal in the process of drinking water production. *Chemosphere* **2008**, *71*, 97−106.
(12) Tobin, R. S.; Smith, D. K.; Lindsay, J. A. Effects of activated carbon and bacteriostatic filters on microbiological quality of drinking water. *Appl. Environ. Microbiol.* **1981**, *41*, 646−651.
(13) Gupta, V. K.; Gupta, B.; Rastogi, A.; Agarwal, S.; Nayak, A. Pesticides removal from waste water by activated carbon prepared from waste rubber tire. *Water Res.* **2011**, *45*, 4047−4055.
(14) Joshi, R.; Carbone, P.; Wang, F. C.; Kravets, V. G.; Su, Y.; Grigorieva, I. V.; Wu, H.; Geim, A. K.; Nair, R. R. Precise and ultrafast molecular sieving through graphene oxide membranes. *Science* **2014**, *343*, 752−754.
(15) Pendolino, F.; Armata, N. Graphene oxide in environmental remediation process. *Springer* **2017**, 5−21.
(16) Mi, B. Graphene oxide membranes for ionic and molecular sieving. *Science* **2014**, *343*, 740−742.
(17) Abraham, J.; Vasu, K. S.; Williams, C. D.; Gopinadhan, K.; Su, Y.; Cherian, C. T.; Dix, J.; Prestat, E.; Haigh, S. J.; Grigorieva, I. V.; et al. Tunable sieving of ions using graphene oxide membranes. *Nat. Nanotechnol.* **2017**, *12*, 546.
(18) Gao, W. The chemistry of graphene oxide. In *Graphene oxide*; Springer, 2015; pp 61−95.
(19) Zhu, Y.; Murali, S.; Cai, W.; Li, X.; Suk, J. W.; Potts, J. R.; Ruoff, R. S. Graphene and graphene oxide: synthesis, properties, and applications. *Adv. Mater.* **2010**, *22*, 3906−3924.
(20) Fraga, T. J.; Carvalho, M. N.; Ghislandi, M. G.; Motta Sobrinho, M. A. D. Functionalized graphene-based materials as innovative adsorbents of organic pollutants: A concise overview. *Braz. J. Chem. Eng.* **2019**, *36*, 1−31.
(21) Yan, F.; Yu, C.; Zhang, B.; Zou, T.; Zhao, H.; Li, J. Preparation of freestanding graphene-based laminar membrane for clean-water intake via forward osmosis process. *RSC Adv.* **2017**, *7*, 1326−1335.
(22) Wei, Y.; Zhang, Y.; Gao, X.; Ma, Z.; Wang, X.; Gao, C. Multilayered Graphene Oxide Membrane for Water Treatment: A Review. *Carbon* **2018**, *139*, 964−981.
(23) Guo, S.; Zhang, G.; Guo, Y.; Yu, J. C. Graphene oxide-Fe_2O_3 hybrid material as highly efficient heterogeneous catalyst for degradation of organic contaminants. *Carbon* **2013**, *60*, 437−444.
(24) Sun, H.; Liu, S.; Zhou, G.; Ang, H. M.; Tadé, M. O.; Wang, S. Reduced graphene oxide for catalytic oxidation of aqueous organic pollutants. *ACS Appl. Mater. Interfaces* **2012**, *4*, 5466−5471.
(25) Spyrou, K.; Potsi, G.; Diamanti, E. K.; Ke, X.; Serestatidou, E.; Verginadis, I. I.; Velalopoulou, A. P.; Evangelou, A. M.; Deligiannakis, Y.; Van Tendeloo, G.; Gournis, D.; Rudolf, P. Towards Novel Multifunctional Pillared Nanostructures: Effective Intercalation of Adamantylamine in Graphene Oxide and Smectite Clays. *Adv. Funct. Mater.* **2014**, *24*, 5841−5850.
(26) Niu, Z.; Liu, L.; Zhang, L.; Chen, X. Porous graphene materials for water remediation. *Small* **2014**, *10*, 3434−3441.
(27) Adeleye, A. S.; Conway, J. R.; Garner, K.; Huang, Y.; Su, Y.; Keller, A. A. Engineered nanomaterials for water treatment and remediation: costs, benefits, and applicability. *Chem. Eng. J.* **2016**, *286*, 640−662.
(28) Pei, Z.; Li, L.; Sun, L.; Zhang, S.; Shan, X.-q.; Yang, S.; Wen, B. Adsorption characteristics of 1, 2, 4-trichlorobenzene, 2, 4, 6-trichlorophenol, 2-naphthol and naphthalene on graphene and graphene oxide. *Carbon* **2013**, *51*, 156−163.
(29) Yang, Z.; Yan, H.; Yang, H.; Li, H.; Li, A.; Cheng, R. Flocculation performance and mechanism of graphene oxide for removal of various contaminants from water. *Water Res.* **2013**, *47*, 3037−3046.
(30) Ivashenko, O.; Logtenberg, H.; Areephong, J.; Coleman, A. C.; Wesenhagen, P. V.; Geertsema, E. M.; Heureux, N.; Feringa, B. L.; Rudolf, P.; Browne, W. R. Remarkable stability of high energy conformers in self-assembled monolayers of a bistable electro-and photoswitchable overcrowded alkene. *J. Phys. Chem. C* **2011**, *115*, 22965−22975.
(31) Moulder, J. F.; Stickle, W. F.; Sobol, P. E. *Handbook of X-ray Photoelectron Spectroscopy*; Physical Electronics Division, Perkin-Elmer Corp., Eden Prairie, MN, 1993.
(32) Shirley, D. A. High-resolution X-ray photoemission spectrum of the valence bands of gold. *Phys. Rev. B* **1972**, *5*, 4709.
(33) Spyrou, K.; Calvaresi, M.; Diamanti, E. K.; Tsoufis, T.; Gournis, D.; Rudolf, P.; Zerbetto, F. Graphite oxide and aromatic amines: Size matters. *Adv. Funct. Mater.* **2015**, *25*, 263−269.
(34) Flores Céspedes, F.; Villafranca Sánchez, M.; Pérez Garcia, S.; Fernández Pérez, M. Modifying sorbents in controlled release formulations to prevent herbicides pollution. *Chemosphere* **2007**, *69*, 785−794.
(35) Flores-Céspedes, F.; Daza-Fernández, I.; Villafranca-Sánchez, M.; Fernández-Pérez, M.; Morillo, E.; Undabeytia, T. Lignin and ethylcellulose in controlled release formulations to reduce leaching of chloridazon and metribuzin in light-textured soils. *J. Hazard. Mater.* **2018**, *343*, 227−234.
(36) Freundlich, H. Over the adsorption in solution. *J. Phys. Chem.* **1906**, *57*, 1100−1107.

https://dx.doi.org/10.1021/acsestwater.0c00037
ACS EST Water 2021, 1, 157−166

(37) Langmuir, I. The constitution and fundamental properties of solids and liquids. Part I. Solids. *J. Am. Chem. Soc.* **1916**, *38*, 2221−2295.
(38) Park, S.; Ruoff, R. S. Chemical methods for the production of graphenes. *Nat. Nanotechnol.* **2009**, *4*, 217−224.
(39) Sánchez-Martín, M. J.; Sáanchez-Camazano, M. Adsorption of chloridazon by soils and their components. *Weed Sci.* **1991**, *39*, 417−422.
(40) Giles, C. H.; Smith, D.; Huitson, A. A general treatment and classification of the solute adsorption isotherm. I. Theoretical. *J. Colloid Interface Sci.* **1974**, *47*, 755−765.
(41) Yan, F.; Spyrou, K.; Thomou, E.; Kumar, S.; Cao, H.; Stuart, M. C.; Pei, Y.; Gournis, D.; Rudolf, P. Smectite clay pillared with copper complexed polyhedral oligosilsesquioxane for adsorption of chloridazon and its metabolites. *Environ. Sci.: Nano* **2020**, *7*, 424.
(42) González-Pradas, E.; Villafranca-Sánchez, M.; Socías-Viciana, M.; Cantos-Molina, A.; Ureña-Amate, M. D. Removal of chloridazon from water by kerolite/stevensite and bentonite: a comparative study. *J. Chem. Technol. Biotechnol.* **2000**, *75*, 1135−1140.
(43) González-Pradas, E.; Socías-Viciana, M.; Urena-Amate, M.; Cantos-Molina, A.; Villafranca-Sánchez, M. Adsorption of chloridazon from aqueous solution on heat and acid treated sepiolites. *Water Res.* **2005**, *39*, 1849−1857.
(44) Socias-Viciana, M.; Tévar de Fez, J.; Urena-Amate, M.; Gonzalez-Pradas, E.; Fernandez-Perez, M.; Flores-Cespedes, F. Removal of chloridazon by natural and ammonium kerolite samples. *Appl. Surf. Sci.* **2006**, *252*, 6053−6057.
(45) Ureña-Amate, M. D.; Socías-Viciana, M. M.; González-Pradas, E.; Cantos-Molina, A.; Villafranca-Sánchez, M.; López-Teruel, C. Adsorption of chloridazon from aqueous solution on modified kerolite-rich materials. *J. Environ. Sci. Health, Part B* **2008**, *43*, 141−150.
(46) Gérard, M.-C.; Barthélemy, J.-P. An assessment methodology for determining pesticides adsorption on granulated activated carbon. *Biotechnol., Agron., Soc. Environ.* **2003**, *7*, 79−85.
(47) El-Said, W. A.; El-Khouly, M. E.; Ali, M. H.; Rashad, R. T.; Elshehy, E. A.; Al-Bogami, A. S. Synthesis of mesoporous silica-polymer composite for the chloridazon pesticide removal from aqueous media. *J. Environ. Chem. Eng.* **2018**, *6*, 2214−2221.
(48) Kozyatnyk, I.; Yacout, D. M.; Van Caneghem, J.; Jansson, S. Comparative environmental assessment of end-of-life carbonaceous water treatment adsorbents. *Bioresour. Technol.* **2020**, *302*, 122866.
(49) Cossutta, M.; McKechnie, J.; Pickering, S. J. A comparative LCA of different graphene production routes. *Green Chem.* **2017**, *19*, 5874−5884.
(50) Alves, M.; Rodrigues, A.; Cossutta, F.; Freitas, P.; Cruz, J.; Rocha, M.; Cruz, M.; Fonseca, T. Atrial Fibrillation Screening in Elderly Patients With Risk Factors for Stroke. The Value of Prolonged Cardiac Monitoring. *Cardiology and Cardiovascular Medicine* **2019**, *4*, 021−027.
(51) Yan, H.; Wu, H.; Li, K.; Wang, Y.; Tao, X.; Yang, H.; Li, A.; Cheng, R. Influence of the surface structure of graphene oxide on the adsorption of aromatic organic compounds from water. *ACS Appl. Mater. Interfaces* **2015**, *7*, 6690−6697.
(52) Wang, F.; Haftka, J. J.-H.; Sinnige, T. L.; Hermens, J. L.; Chen, W. Adsorption of polar, nonpolar, and substituted aromatics to colloidal graphene oxide nanoparticles. *Environ. Pollut.* **2014**, *186*, 226−233.
(53) Wang, J.; Chen, Z.; Chen, B. Adsorption of polycyclic aromatic hydrocarbons by graphene and graphene oxide nanosheets. *Environ. Sci. Technol.* **2014**, *48*, 4817−4825.
(54) Björk, J.; Hanke, F.; Palma, C.-A.; Samori, P.; Cecchini, M.; Persson, M. Adsorption of aromatic and anti-aromatic systems on graphene through π-π stacking. *J. Phys. Chem. Lett.* **2010**, *1*, 3407−3412.
(55) Wang, X.; Huang, S.; Zhu, L.; Tian, X.; Li, S.; Tang, H. Correlation between the adsorption ability and reduction degree of graphene oxide and tuning of adsorption of phenolic compounds. *Carbon* **2014**, *69*, 101−112.
(56) Yan, H.; Tao, X.; Yang, Z.; Li, K.; Yang, H.; Li, A.; Cheng, R. Effects of the oxidation degree of graphene oxide on the adsorption of methylene blue. *J. Hazard. Mater.* **2014**, *268*, 191−198.
(57) Roos, M.; Künzel, D.; Uhl, B.; Huang, H. H.; Brandao Alves, O.; Hoster, H. E.; Gross, A.; Behm, R. J. Hierarchical interactions and their influence upon the adsorption of organic molecules on a graphene film. *J. Am. Chem. Soc.* **2011**, *133*, 9208−9211.
(58) Zhou, Y.; Apul, O. G.; Karanfil, T. Adsorption of halogenated aliphatic contaminants by graphene nanomaterials. *Water Res.* **2015**, *79*, 57−67.
(59) Spyrou, K.; Rudolf, P. An introduction to graphene. *Functionalization of graphene* **2014**, 1−20.
(60) Kim, J.; Cote, L. J.; Kim, F.; Yuan, W.; Shull, K. R.; Huang, J. Graphene oxide sheets at interfaces. *J. Am. Chem. Soc.* **2010**, *132*, 8180−8186.
(61) Meylan, W. M.; Howard, P. H.; Boethling, R. S. Improved method for estimating water solubility from octanol/water partition coefficient. *Environ. Toxicol. Chem.* **1996**, *15*, 100−106.
(62) Miller, M. M.; Wasik, S. P.; Huang, G. L.; Shiu, W. Y.; Mackay, D. Relationships between octanol-water partition coefficient and aqueous solubility. *Environ. Sci. Technol.* **1985**, *19*, 522−529.
(63) Chen, X.; Chen, B. Macroscopic and spectroscopic investigations of the adsorption of nitroaromatic compounds on graphene oxide, reduced graphene oxide, and graphene nanosheets. *Environ. Sci. Technol.* **2015**, *49*, 6181−6189.
(64) Chen, D.; Feng, H.; Li, J. Graphene oxide: preparation, functionalization, and electrochemical applications. *Chem. Rev.* **2012**, *112*, 6027−6053.
(65) Dong, F.; Wu, L.; Sun, Y.; Fu, M.; Wu, Z.; Lee, S. Efficient synthesis of polymeric g-C_3N_4 layered materials as novel efficient visible light driven photocatalysts. *J. Mater. Chem.* **2011**, *21*, 15171−15174.
(66) Ashwell, G. J.; Williams, A. T.; Barnes, S. A.; Chappell, S. L.; Phillips, L. J.; Robinson, B. J.; Urasinska-Wojcik, B.; Wierzchowiec, P.; Gentle, I. R.; Wood, B. J. Self-Assembly of Amino-Thiols via Gold-Nitrogen Links and Consequence for in situ Elongation of Molecular Wires on Surface-Modified Electrodes. *J. Phys. Chem. C* **2011**, *115*, 4200−4208.
(67) Lee, J. Y.; Bashur, C. A.; Goldstein, A. S.; Schmidt, C. E. Polypyrrole-coated electrospun PLGA nanofibers for neural tissue applications. *Biomaterials* **2009**, *30*, 4325−4335.
(68) Kemnitz, C. R.; Loewen, M. J. Amide Resonance" Correlates with a Breadth of C-N Rotation Barriers. *J. Am. Chem. Soc.* **2007**, *129*, 2521−2528.
(69) Li, D.; Muller, M. B.; Gilje, S.; Kaner, R. B.; Wallace, G. G. Processable Aqueous Dispersions of Graphene Nanosheets. *Nat. Nanotechnol.* **2008**, *3*, 101−105.
(70) Konkena, B.; Vasudevan, S. Understanding aqueous dispersibility of graphene oxide and reduced graphene oxide through pKa measurements. *J. Phys. Chem. Lett.* **2012**, *3*, 867−872.
(71) Dai, M. The effect of zeta potential of activated carbon on the adsorption of dyes from aqueous solution: I. The adsorption of cationic dyes: methyl green and methyl violet. *J. Colloid Interface Sci.* **1994**, *164*, 223−228.
(72) Ersan, G.; Apul, O. G.; Perreault, F.; Karanfil, T. Adsorption of organic contaminants by graphene nanosheets: A review. *Water Res.* **2017**, *126*, 385−398.
(73) Wang, H.; Hu, B.; Gao, Z.; Zhang, F.; Wang, J. Emerging role of graphene oxide as sorbent for pesticides adsorption: experimental observations analyzed by molecular modeling. *J. Mater. Sci. Technol.* **2020**, DOI: 10.1016/j.jmst.2020.02.033.